Two-Dimensional Penning Ionization Electron Spectroscopy of Adamantanes and Cyclohexanes: Electronic Structure of Adamantane, *1*-Chloroadamantane, Cyclohexane, and Chlorocyclohexane and Interaction Potential with He*(2^3S)

Shan Xi Tian, Naoki Kishimoto, and Koichi Ohno*

Department of Chemistry, Graduate School of Science, Tohoku University, Aramaki, Aoba-ku, Sendai 980-8578, Japan

Received: November 20, 2001; In Final Form: May 6, 2002

The electronic structures of adamantane, *1*-chloroadamantane, cyclohexane, and chlorocyclohexane and their interaction potentials with He*(2^3S) metastable atoms are studied by two-dimensional (collision- and electron-energy-resolved) Penning ionization electron spectroscopy and model potential calculations. The model potential calculations are performed for the target-Li system based on a well-known resemblance between a metastable excited He*(2^3S) atom and a ground-state Li(2^2S) atom. Assignments of the electron spectra are made on the basis of ab initio and outer-valence Green's function calculations. Strong repulsive interactions between the saturated hydrocarbons and the metastable atom and strength sequence $\sigma_{CC} > \sigma_{CH}$ observed experimentally are consistent with the anisotropic potential calculations. It is noted that attractive interaction in the region where lone-pair n_{Cl} electrons are distributed for *1*-chloroadamantane is weaker than that for chlorocyclohexane, because of the stronger steric shielding effect by the larger adamantane skeleton. Through comparison with the previous results on the saturated chloro-hydrocarbons, we find that the attractive interaction around the n_{Cl} electron distribution does not become stronger as the energy level of the highest occupied molecular orbital becomes higher, which is the result of competition between effects of low exterior electron distributions and high energy levels.

I. Introduction

In the chemiionization process known as Penning ionization,[1−5] a molecule M collides with a metastable atom A* having an excitation energy (E_A) much larger than the lowest ionization potential (IP) of the molecule. Penning ionization electron spectroscopy is an experimental technique used to detect the kinetic energy of the electron ejected in the ionization process, in which the ground-state atom A and the ionic states of the molecule M_i^+ are the coproducts as follows:[3−5]

$$M + A^* \rightarrow A + M_i^+ + e^- \quad (1)$$

The exact kinetic energy of the ejected electron (E_e^i) is equal to the difference between two potential energy functions, the incoming M + A* interaction potential V^* and the outgoing A + M_i^+ interaction potential V_i^+. Both are functions of the internuclear distance R between the metastable atom and the molecule, and the kinetic energy E_e^i of Penning electron is determined by

$$E_e^i(R) = V^*(R) - V_i^+(R) = E_A - IP_i + \Delta E_i(R) \quad (2)$$

where ΔE_i is the peak shift in Penning ionization electron spectrum (PIES) with respect to the peak positions observed in ultraviolet photoelectron spectrum (UPS). Usually, ΔE_i is negative if the incoming interaction potential is attractive and positive if this potential is repulsive. Partial ionization cross-sections or branching ratios of the different ionic states are usually dependent on the electron distribution of respective ionized molecular orbitals.[6] As molecular orbitals (MO) are highly anisotropic with electron densities more or less localized on a certain part of the molecule, collision energy (E_c) dependence of partial ionization cross-sections (CEDPICS) has negative or positive slopes, reflecting the anisotropy of the interaction potential V^*. Velocity-controlled supersonic metastable atom beams have been utilized to observe Penning ionization spectra for some atoms and small molecules.[7−9] In our laboratory, an ionic-state-resolved PIES experiment combined with a time-of-flight (TOF) technique has been developed as two-dimensional (collision- and electron-energy-resolved) Penning ionization electron spectroscopy[10−20] which can be used to obtain collision-energy resolved Penning ionization electron spectra (CERPIES) and CEDPICS for the target molecule.

The two-dimensional (2D) PIES measurements allow us to investigate the anisotropic potential energy surface around the target molecule by analyzing CEDPICS. The interaction potentials between metastable He*(2^3S) atoms and some saturated[13,14] or unsaturated hydrocarbons[15−20] have been studied. In particular, a 2D-PIES study of cyclopropanes[14] indicates that the potential is repulsive near the saturated carbon−carbon (C−C) and carbon−hydrogen (C−H) bonds and attractive near the substituted group with lone-pair electrons, which is in agreement with the model calculations of interaction potentials using Li(2^2S) atom. As is well-known, the shape of velocity dependence of the total scattering cross section of He*(2^3S) with He, Ar, and Kr is very similar to that of Li(2^2S),[21] and interaction well-depths and the location of potential wells have been found to be very similar for interactions of various targets with He*-

* To whom correspondence should be addressed.

10.1021/jp014302e CCC: $22.00
Published on Web 06/21/2002

(2^3S) and Li(2^2S).[2,11,22−23] This similarity between He*(2^3S) and Li(2^2S) is usually employed to compare the computationally more feasible M−Li potentials with the experimental results for M−He*(2^3S) interactions.[13−20]

There are a number of merits to CERPIES in comparison with other electron spectroscopy for studying electronic structures and particularly for molecular interactions. First, it differs from photoelectron spectrum (PES) in that certain band intensities are enhanced or lowered in PIES, which is helpful in recognizing MO characters and assigning spectral features.[6,24] Second, satellite bands are more frequently observed in PIES than in PES.[12,25] In particular, CERPIES combined with theoretical calculations allow us to determine the ionic states related to the satellites.[26] As yet, there are no accurate theories for describing molecular interactions. Fortunately, the experimental PIES technique is a powerful means that enables us to obtain information to develop such theories. Through analyzing CEDPICS, it is possible to determine whether the interactions around the target molecule are attractive or repulsive.

Several groups have used collision-energy-resolved techniques for Penning ionization reaction to investigate the anisotropic interaction around chlorine (Cl) atom with metastable atoms.[27−33] Photoemission cross sections for CH radicals produced by collision of He*(2^3S) atoms with CH_3X (X = H, Cl, Br, and I) have been studied in the collision energy range of 120−210 meV, where the sum of these cross sections was correlated well with dipole-induced interaction of He*(2^3S) with the targets, in particular, the approaches perpendicular to the C−Cl bond axis were found to be governed by an attractive interaction.[27] However, Albert et al. suggested that the attractive interaction was located around an angle of 45° with respect to the C−Cl bond axis in the Ne*($^3P_{2,0}$)−CH_3Cl interaction system,[28] which shows that the simple correlation with the local dipole direction (C−Cl bond axis) does not always hold. The reaction of Ar*-($^3P_{2,0}$) with $CHCl_3$ was studied by Yamato et al. using a combination of a TOF technique and an electric hexapole orientation technique, where the authors presented a correlation between collision energy and the steric effect.[29] In our laboratory, attractive interaction potentials around the Cl atom have been studied for $(CH_3)_3CCl$,[13] chlorobenzene;[30] *trans*-, *cis*-, and *iso*-dichloroethlenes;[31] vinyl chloride;[16,32] and C_2H_5Cl,[33] using the 2D-PIES technique.

In the present study, the 2D-PIES technique including CERPIES and CEDPICS is applied to the investigation of the electronic structures of adamantane ($C_{10}H_{16}$), cyclohexane (C_6H_{12}), and their chloro-derivatives and interactions with He*-(2^3S) atoms. Adamantane is the simplest polycyclic saturated hydrocarbon with a cage-like skeleton characteristic of the diamond lattice, and cyclohexane is a saturated six-carbon cyclic hydrocarbon that may be considered as a structural unit of adamantane (see Scheme 1). Adamantane is the parent molecule of drugs such as the bottle-able carbene[34] and its derivative, adamantine, has been used in the therapy, most notably in chemoprophylaxis, for influenza A, and in the treatment of human Parkinsonian disease.[35] Cyclohexanes are commonly used as organic solvents in chemical technology.[36] Medical applications and solution capability come from the characteristic molecular interactions, and the molecular chemical reactivity is closely related to the electronic structures of the frontier MOs. Recently, Litvinyuk et al. reported the momentum profiles of the outer-valence orbitals of molecular adamantane, adamantine, and urotropine, using (e,2e) electron momentum spectroscopy (EMS).[37] The He I and He II UPS and X-ray photoelectron spectra (XPS) of molecular adamantanes[38] and cyclohexanes[39]

SCHEME 1: Molecular Structures

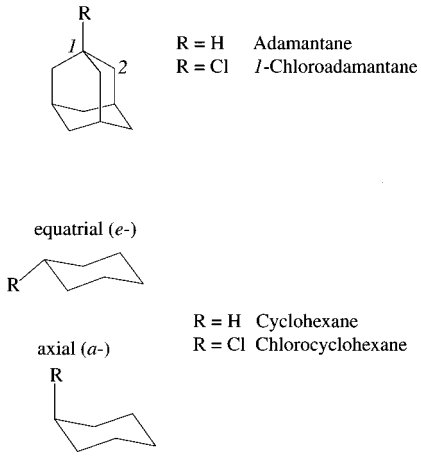

were recorded almost 30 years ago, in which interest was focused on the IPs of the highest occupied molecular orbitals (HOMO) of the derivatives. The effects of substitution on the molecular electronic structure and steric interactions with He*-(2^3S) atom are focus of the present research.

II. Experimental Section

Details of the experimental apparatus have been reported elsewhere.[10−13] Metastable atoms of He*(2^1S, 2^3S) were produced by a discharged nozzle source with a tantalum hollow cathode. The He*(2^1S) component was quenched by a water-cooled helium discharge lamp. He I resonance photons (584 Å, 21.22 eV) produced by a discharge in pure helium gas were used to obtain UPS. The kinetic energies of the electrons ejected in Penning ionization or photoionization were determined by a hemispherical electrostatic deflection type analyzer using an electron collection angle 90° to the incident He*(2^3S) beam axis or He I light beam axis. The energy resolution of the electron analyzer was estimated to be 80 meV from the full width at half-maximum (fwhm) of the Ar^+($^2P_{3/2}$) peak in the He I UPS for the energy-higher-resolution PIES and UPS measurements of the samples; for the CEDPICS measurements, the resolution was lowered to 250 meV in order to obtain higher electron counting rates. The transmission efficiency curves of the electron energy analyzer for both of these two modes were determined by comparing our UPS data of some molecules with those obtained by Gardner and Samson[40] and Kimura et al.[41] The calibration of the electron energy scale was made with reference to the lowest ionic state of molecule nitrogen mixed with the sample molecule in He I UPS (E_e = 5.639 eV) and He*(2^3S) PIES (E_e = 4.292 eV) including a peak energy shift of 50 meV and the difference between the metastable excitation energy and the lowest IP.

For the collision-energy-resolved measurements of Penning ionization, the metastable He*(2^3S) beam was modulated by a pseudorandom chopper rotating at ca. 370 Hz and then introduced into a reaction cell located at 504 mm downstream from the chopper disk. Time dependent electron signals for each kinetic electron energy E_e were recorded with scanning electron energies of a 40 meV step, and the dwell time for the TOF measurements was 3μs. The two-dimensional data as functions of E_e and time t were stored in a 2MB RAM. Two-dimensional spectra $I_e(E_e,t_{TOF})$, functions of E_e and TOF, can lead to $I_e(E_e,v_{He}^*)$, functions of E_e and the velocity of He* (v_{He}^*) and then to the two-dimensional Penning ionization cross-section

$\sigma(E_e,v_r)$ using the equations

$$\sigma(E_e,v_r) = c\{I_e(E_e,v_{He^*})/I_{He^*}(v_{He^*})\}(v_{He^*}/v_r) \quad (3)$$

$$v_r = [v_{He^*}{}^2 + 3kT/M]^{1/2} \quad (4)$$

where c is a constant, v_r is the relative velocity averaged over the velocity of the target molecule, k is the Boltzmann constant, and T and M are the gas temperature and mass of target molecule, respectively. The velocity distribution $I_{He^*}(v_{He^*})$ of the He* beam was determined by monitoring secondary electrons emitted from the inserted stainless steel plate. Finally, $\sigma(E_e,v_r)$ was normalized by $I_{He^*}(v_{He^*})$ and converted to $\sigma(E_e,E_c)$, functions of E_e and E_c, using the relation

$$E_c = \mu v_r{}^2/2 \quad (5)$$

where μ is the reduced mass of the system. The CEDPICS were obtained from $\sigma(E_e,E_c)$ data within an appropriate range of E_e (typically the fwhm of the respective band) to avoid the effect of neighboring bands. The CEDPIES were cut at the two E_c (85 and 250 meV) from $\sigma(E_e,E_c)$ data with some width.

Adamantane (99%+) and *1*-chloroadamantane (99%+) were purchased from Aldrich, and cyclohexane (99%+) and chlorocyclohexane (99%+) were purchased from Wako Pure Chemical Industries Ltd. They were used after several freeze−pump−thawed cycles. Adamantanes have high melting points (adamantane, 209∼212 °C; *1*-chloroadamantane, 165∼166 °C) yet sublime at room temperature. Cyclohexane and chlorocyclohexane are liquid at room temperature. The powder or liquid sample was contained in a Pyrex tube out of the chamber during the experiments, and the Pyrex tube was connected with a steel tube inserted into the reaction cell in the chamber. The volatility of adamantanes and cyclohexanes at room temperature was high enough to create a sufficient concentration of target molecules in the gas phase, and the ambient pressure was controlled at ca. 2×10^{-5} Torr.

III. Calculations

The geometrical parameters of the molecular adamantane ($C_{10}H_{16}$), *1*-chloroadamantane (*1*−$C_{10}ClH_{15}$), cyclohexane (C_6H_{12}), and chlorocyclohexane (C_6ClH_{11}) were optimized with T_d, C_{3v}, D_{3d}, and C_s symmetries, respectively, at the hybrid density functional B3LYP/6-311++G** level of theory. The two conformers of C_6ClH_{11}, the equatorial (*e*-) and the axial (*a*-), were optimized and found to be of ca. 3 kJ/mol energetic difference in the gas phase. In the electron density contour maps obtained by Hartree−Fock self-consistent-field (HF−SCF) calculations with the 6-31+G* basis set, thick solid curves indicate the repulsive molecular surface approximated by atomic spheres of van der Waals radii ($r_C = 1.7$ Å, $r_H = 1.2$ Å, and $r_{Cl} = 1.8$ Å).[42] The IP values were also calculated for assignments in the He I UPS and PIES by the outer-valence Green's function (OVGF) method[43] with the 6-31+G(d,p) for C_6H_{12} and C_6ClH_{11} and the 4-31G for $C_{10}H_{16}$ and *1*-$C_{10}ClH_{15}$.

Interaction potential calculations with Li(2^2S) atom, $V^*(R)$ (where R is defined in the captions of the related figures), were performed at the unrestricted second-order Møller−Plesset perturbation (UMP2) level of theory using the 4-31G(d) basis set with scanning R values and the geometrical parameters of the targets fixed at the previously optimized values. Spin-contamination is negligible for these calculations. The present calculations of interaction potentials and IP values were performed with Gaussian 98.[44]

It is well-known that the relative intensity of bands in PIES can be successfully compared with the exterior electron density (EED) for individual MOs,[6,45−47] and EED values are a kind of measurements of how far electron distributions expand outside a molecular boundary. In a PIES study, this boundary is defined by the molecular surface which is usually estimated by placing a sphere with an effective radius (e.g., van der Waals radius) on each atom position. EED for each spatial MO wave function φ_i can be expressed by

$$(EED)_i = \int_\Omega |\varphi_i(r)|^2 \, dr \quad (6)$$

where r runs through the region Ω outside the repulsive molecular surface. The exterior region Ω is a sum of the subspace Ω_a which is a region made up of points whose nearest molecular surface belongs to the *a* atom.[48] Moreover, MO wave functions are usually described in terms of basis functions using a linear combination of atomic orbitals (LCAO). Therefore, an EED value of the atom a for the *i*th MO can be obtained using the following expression:[48c]

$$(EED)_{ia} = \int_{\Omega_a} |\varphi_i(r)|^2 \, dr$$

$$\Omega = \sum_a \Omega_a \quad (7)$$

The EED concept and these two formula are very helpful to analyze substitution effects on electronic structures and interactions with a He*(2^3S) atom. So we performed EED calculations for *1*-$C_{10}ClH_{15}$ and *e*-C_6ClH_{11} as well as C_2ClH_5 (C_s) and C_4ClH_9 (C_{3v}), using the HF/6-31+G* wave functions.

IV. Results

The He I UPS and He*(2^3S) PIES of $C_{10}H_{16}$, *1*-$C_{10}ClH_{15}$, C_6H_{12}, and C_6ClH_{11} are shown in Figures 1-4, respectively. The electron energy scales for PIES are shifted 1.40 eV relative to those for UPS by the difference in the excitation energies between the He I photon (21.22 eV) and the He*(2^3S) atom (19.82 eV). Because of the Jahn−Teller effect and Franck−Condon effect, the ionization bands of highly degenerate states of adamantane are diffuse and overlapping. Assignments given in Figures 1−4 and Tables 1−4 were made on the basis of the IP values and the orbital energy levels obtained at the OVGF and HF/6-311++G** levels. The EMS study has drawn the conclusion that the Hartree−Fock as well as density-functional calculations with the 6-311++G** basis set are in good agreement with the experimental momentum profiles.[37] The HF/6-311++G** calculations of this work gave the electron configuration of adamantane as $(core)^{32}(4t_2)^6(4a_1)^2(5a_1)^2(5t_2)^6(1t_1)^6(6t_2)^6(2t_1)^6(3e)^4(7t_2)$.[6]

In the earlier spectra of C_6H_{12}, the molecular structure was assumed to be a D_{6h} symmetrical one,[39d] whereas Kimura et al. used the D_{3d} symmetry.[41] Here we adopted the latter for the present assignments. For the C_6ClH_{11} spectra in Figure 4, the orbitals of the predominant isomer *e*-C_6ClH_{11} were used for assignments except for the band labels in the parentheses that are contributions of *a*-C_6ClH_{11}.

Figures 5−8 show the CERPIES obtained from the 2D spectra of $C_{10}H_{16}$, *1*-$C_{10}ClH_{15}$, C_6H_{12}, and C_6ClH_{11}, respectively. Hot spectra at the higher collision energy ca. 250 meV are shown by dotted curves, and cold spectra at the lower collision energy ca. 85 meV are shown by solid curves.

Log σ vs log E_c plots of the CEDPICS in a collision energy range of 70−300 meV are presented in Figures 9−12 for $C_{10}H_{16}$,

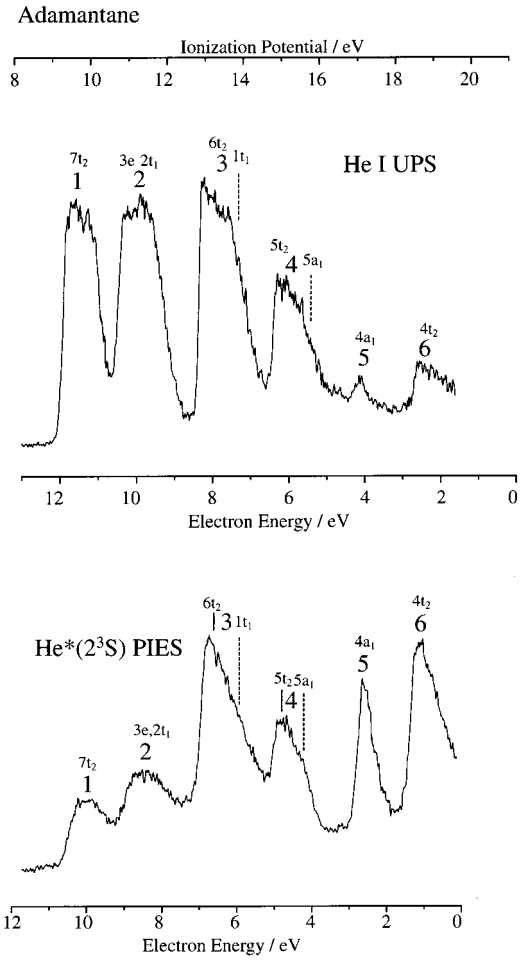

Figure 1. He I ultraviolet photoelectron spectrum (UPS) and He*-(2^3S) Penning ionization electron spectrum (PIES) of adamantane.

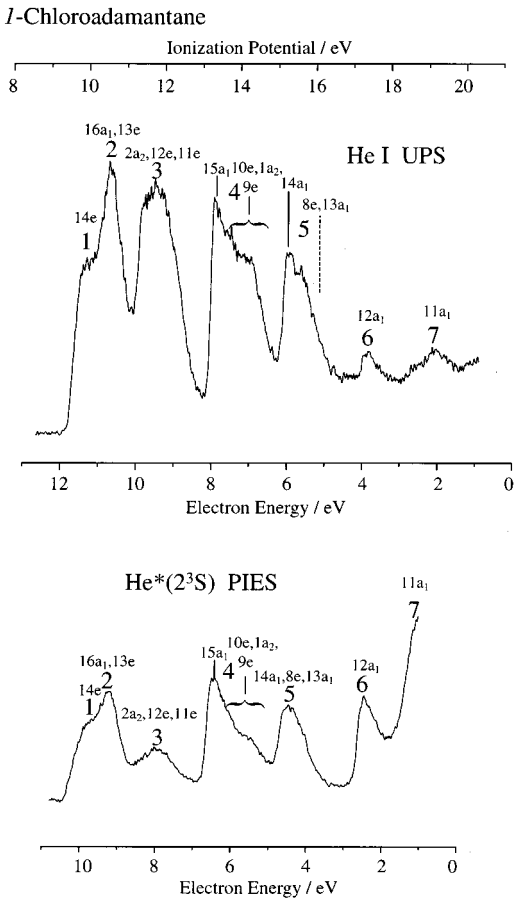

Figure 2. He I UPS and He*(2^3S) PIES of *1*-chloroadamantane.

1-$C_{10}ClH_{15}$, C_6H_{12}, and C_6ClH_{11}, respectively. The calculated electron density maps are shown in proper directions in order to grasp most effective directions of the ionization or effective access direction of the He* atom. Different maps are also presented for the degenerate orbitals and the C_6ClH_{11} isomers. In Figure 10, the second density maps of the 14e, 13e, 12e, 11e, and 10e orbitals and the map of the $14a_1$ orbital are plotted on plane b′ at a distance of 0.80 Å from the molecular nodal plane b of *1*-$C_{10}ClH_{15}$. The electron density distributionsof the $2a_2$ and $1a_2$ orbitals of *1*-$C_{10}ClH_{15}$ are plotted on a top-viewed plane a in Figure 10, and those of the $4a_{1g}$ and $1a_{1u}$ orbitals of C_6H_{12} are plotted on plane b in Figure 11. In Figure 12, the electron density of each orbital except for 9a″, 8a″, 7a″, 16a′, 6a″, and 12a′ is plotted on the molecular plane a.

Figures 13−16 show the calculated profiles of the interaction potential energies between a ground-state Li atom and $C_{10}H_{16}$, *1*-$C_{10}ClH_{15}$, C_6H_{12}, and C_6ClH_{11}, respectively.

Tables 1−4 summarize the experimental and calculated IPs, experimental peak energy shifts (ΔE), slope parameters of CEDPICS (m), and the assignments of the bands with orbital characters, as well as the IP data available in the previous literatures for comparison. Slope parameters (m) are obtained from the log σ vs log E_c plots in a collision energy range of 70−300 meV by a least-squares fitting method. Vertical and adiabatic (noted with a) IPs are determined from the present He I UPS. The peak energy shifts are obtained as the difference between the peak positions in PIES (E_{PIES}, in electron energy scale) and the *nominal* value (E_0 = difference between the metastable excitation energy and sample IP): $\Delta E = E_{PIES} - E_0$.

SCHEME 2: Correlation Diagram for the Outer Valence Orbitals of Adamantanes and Cyclohexanes

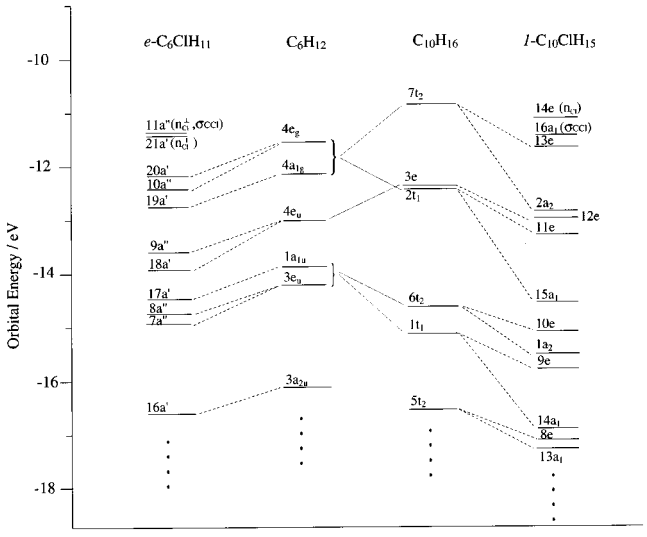

V. Discussion

The electronic spectra for these four molecules adamantane, *1*-chloroadamantane, cyclohexane, and chlorocyclohexane show that bands attributed to the valence orbitals of the high-symmetry molecules split when the symmetries are lowered. Through comparisons of the spectra of adamantane (T_d) and *1*-chloro-

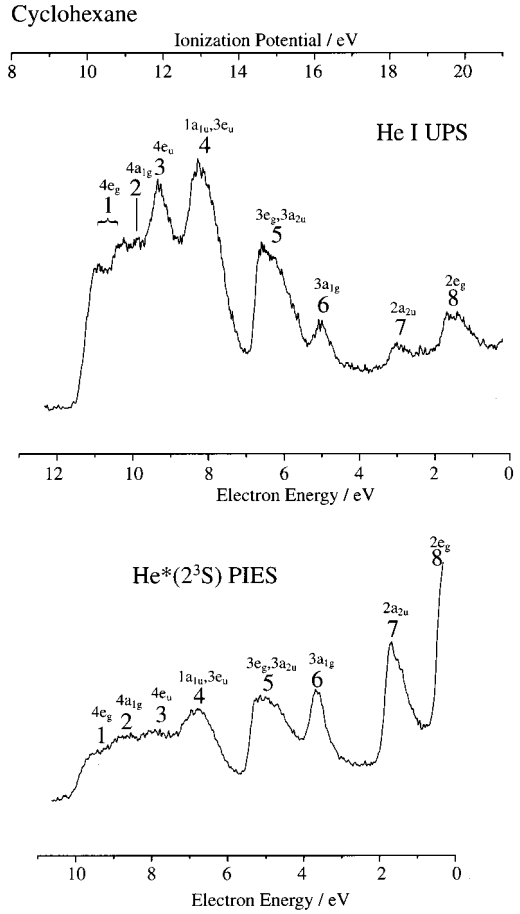

Figure 3. He I UPS and He*(2³S) PIES of cyclohexane.

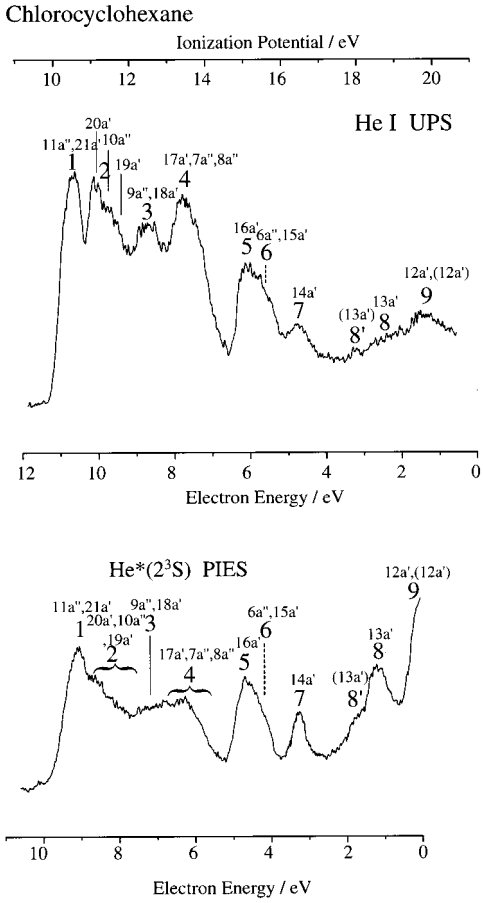

Figure 4. He I UPS and He*(2³S) PIES of chlorocyclohexane.

adamantane (C_{3v}), one can find that the triply degenerate $7t_2$ orbital splits into 13e and $2a_2$, $2t_1$ into 11e and $15a_1$, $6t_2$ into 10e and $1a_2$, $1t_1$ into 9e and $14a_1$, and $5t_2$ into 8e and $13a_1$. For cyclohexane (D_{3d}) and chlorocyclohexane (C_s), the doubly degenerate $4e_g$ splits into 20a′ and 10a″, $4e_u$ into 9a″ and 18a′, $3e_u$ into 7a″ and 8a″, and $3e_g$ into 16a′ and 6a″. A correlation diagram for orbital splitting is shown in Scheme 2. In this work, we assign features in the spectra on the basis of theoretical calculations and PIES characteristics.

In Figures 2 and 4, the first band (14e) of *1*-$C_{10}ClH_{15}$ is weaker than the first band of C_6ClH_{11}, explained as due to stronger steric shielding effect of the larger skeleton of adamantane than that of the cyclohexane ring with respect to the unbonded lone-pair electrons (n_{Cl}). Such shielding of bulky groups has been documented for various compounds including ferrocene,[49a] anilines,[49b] and $Fe(CO)_5$,[49c] and recently, it was also observed for chlorobenzene.[30] This work may be viewed as an extension research for examining the effect of substituting the Cl atom into larger saturated hydrocarbons in comparison with previous results for the saturated chloro-hydrocarbons [$(CH_3)_3CCl$[13] and CH_3CH_2Cl[33]].

A. Adamantane and Cyclohexane. He I and He II spectra of the molecular adamantane have already been obtained,[38] but the orbitals below 2e are not included in the present work because of energy limitations. Six bands can be seen in Figure 1. The first band which has contribution from the HOMO $7t_2$ of $C_{10}H_{16}$ is very broad, because the $7t_2$ orbital is strongly σ_{CC} bonding and the triply degenerate T_2 state formed by removal of a $7t_2$ electron is subject to Jahn−Teller distortions. Because bands 2−4 are composed of two ionic states and also undergo Jahn−Teller effect, the IPs cannot be estimated accurately. However, the observed vertical IPs are generally in agreement with the calculated OVGF data and the (e,2e) experimental values[37a] in Table 1. The HOMO of C_6H_{12} is the doubly degenerate $4e_g$, which is observed as two small split bands in Figure 3. Similar features have been observed for cyclopropane.[14] The outermost orbitals of both $C_{10}H_{16}$ and C_6H_{12} are mainly σ_{CC} bonding, and if C_6H_{12} is considered a structural unit of $C_{10}H_{16}$, we can suppose simply that bands 1 ($7t_2$) and 2 (3e and $2t_1$) of $C_{10}H_{16}$ consist of bands 1 ($4e_g$), 2 ($4a_{1g}$), and 3 ($4e_u$) of C_6H_{12}, as shown in Scheme 2.

In Figure 1, the assignment sequence of band 2 differs from the earlier UPS analyses in which the reverse sequence was assigned[38e] although it cannot be resolved clearly due to Jahn−Teller splitting as well as the Franck−Condon effect. The *p*-type momentum profile of this band observed in the EMS study confirmed that the orbitals 3e and $2t_1$ represent σ_{CC} bonding similar to band 1 ($7t_2$).[37a] Bands 3 and 4 are mainly assigned to σ_{CH} bonding. As shown in the electron density maps in Figure 9, more electrons of σ_{CH} bonding are exposed to the outside of the van der Waals radii than those of σ_{CC} bonding. The band intensity in PIES reveals that the probability of the electron-transfer process is governed by the mutual overlap between the orbital of He* and the target M; it is known that an electron in a molecular orbital is transferred to the inner-vacant orbital of He*, and the excited electron in He* is ejected.[2,6] Therefore, bands 3 and 4 are stronger than bands 1 and 2 in the PIES, as was similarly observed for the C_6H_{12} PIES in Figure 3.

For the C_6H_{12} spectra in Figure 3, Kimura et al. assigned the band with the ionization energy higher than ca. 18 eV having an *s*-orbital character without further information,[41] whereas this band and the higher IP bands were clearly assigned to the valence ionic states (b_{1u}, e_{2g}, e_{1u}, e_{1g}, etc.) using an incorrect

TABLE 1: Band Assignment, Ionization Potentials (IP/eV), Peak Shifts (ΔE/meV), and Slope Parameters (m) for $C_{10}H_{16}$

band	orbital character	IP_{obsd}/eV[a]	IP_{OVGF}/eV (pole strength)	$IP_{(e,2e)}$[b]/eV	ΔE/meV	m
1	$7t_2(\sigma_{CC})$	9.40 (a)				
		9.67	9.50(0.92)	9.7	-100 ± 200	-0.26 ± 0.01
2	$3e(\sigma_{CC})$	(10.86,a)	10.92(0.91)	11.2	-20 ± 100	-0.25 ± 0.01
	$2t_1(\sigma_{CC})$	(11.45)	11.04(0.92)			
3	$6t_2(\pi_{CH},\sigma_{CC})$	13.05(*a*)	13.10(0.91)	13.2	$+10 \pm 20$	-0.20 ± 0.01
	$1t_1(\sigma_{CH})$	(13.44)	13.59(0.91)			
4	$5t_2(\pi_{CH},\sigma_{CC})$	14.87(*a*)	15.01(0.91)	15.1	$+20 \pm 40$	-0.18 ± 0.02
	$5a_1(\sigma_{CH})$	(15.41)	15.45(0.91)			
5	$4a_1(C_{2s},\sigma_{CH})$	17.06	17.12(0.90)	17.0	-30 ± 20	-0.15 ± 0.02
6	$4t_2(C_{2s})$	18.60			(-120 ± 140)	(-0.10 ± 0.03)

[a] The adiabatic ionization potentials are noted as *a* in the parentheses, and the vertical ones are listed without notation. [b] From ref 37a.

TABLE 2: Band Assignment, Ionization Potentials (IP/eV), Peak Shifts (ΔE/meV), and Slope Parameters (m) for *1*-$C_{10}ClH_{15}$

band	orbital character	IP_{obsd}/eV	IP_{OVGF}/eV (pole strength)	ΔE/meV	m
1	14e ($n_{Cl}^{\parallel}$, $n_{Cl}^{\perp}$)	(9.87)	9.66(0.92)	(-200 ± 140)	-0.23 ± 0.03
2	$16a_1(\sigma_{CCl})$	10.52	9.99(0.92)	-120 ± 40	-0.33 ± 0.03
	$13e(n_{Cl},\sigma_{CC})$		10.23(0.92)		
3	$2a_2(\sigma_{CC})$	11.71	11.33(0.92)	-10 ± 80	-0.24 ± 0.03
	$12e(\sigma_{CC},n_{Cl})$		11.41(0.92)		
	$11e(\pi_{CCl})$		11.75(0.92)		
4	$15a_1(\sigma_{CCl})$	13.30	13.05(0.92)	-20 ± 40	-0.22 ± 0.01
	$10e(\sigma_{CH})$		13.44(0.91)		
	$1a_2(\sigma_{CC})$		13.84(0.91)		
	$9e(\pi_{CCl},\sigma_{CH})$		14.06(0.91)		
5	$14a_1(\sigma_{CH},\sigma_{CCl})$	15.26	15.25(0.91)	-100 ± 60	-0.19 ± 0.02
	$8e(\pi_{CH})$		15.40(0.91)		
	$13a_1(C_{2s},\sigma_{CCl})$		15.45(0.91)		
6	$12a_1(Cl_{3s},C_{2s},\sigma_{CH})$	17.26	17.54(0.90)	-100 ± 60	-0.19 ± 0.02
7	$11a_1(C_{2s})$				(-0.16 ± 0.04)

TABLE 3: Band Assignment, Ionization Potentials (IP/eV), Peak Shifts (ΔE/meV), and Slope Parameters (m) for C_6H_{12}

band	orbital character	IP_{obsd}/eV	IP_{OVGF} (pole strength)/eV	$IP_{Koopman}$/eV	ΔE/meV	m
1	$4e_g(\sigma_{CC})$	10.22	10.54(0.91)	11.56	$(+90 \pm 200)$	-0.23 ± 0.03
		10.88				
2	$4a_{1g}(\sigma_{CC})$	11.29	11.31(0.92)	12.15	$(+200 \pm 200)$	-0.28 ± 0.03
3	$4e_u(\sigma_{CC})$	11.89	12.06(0.92)	13.01	-20 ± 80	-0.23 ± 0.03
4	$1a_{1u}(\sigma_{CH})$	12.91	12.52(0.90)	13.90	-80 ± 40	-0.26 ± 0.02
	$3e_u(\sigma_{CH,CC})$	(13.30)		14.23		
5	$3e_g(\sigma_{CH})$	14.60		16.14	-70 ± 40	-0.22 ± 0.02
	$3a_{2u}(\sigma_{CH,CC})$	(15.16)		16.47		
6	$3a_{1g}(\sigma_{CH})$	16.15		17.54	0 ± 40	-0.24 ± 0.01
7	$2a_{2u}(\sigma_{CH}, C_{2s})$	18.10		20.34	-30 ± 40	-0.12 ± 0.03
8	$2e_g(C_{2s})$	19.73		22.49		-0.06 ± 0.03

molecular symmetry (D_{6h}) in an earlier study.[39d] Using the symmetry D_{3d} confirmed by Raman spectra,[50] we assign band 7 to $2a_{2u}$ and band 8 to $2e_g$, with the IPs close to the data (18.06 and 19.49 eV) reported previously.[39d] Here there remain some arguments regarding the vibrational structures of the higher IP bands. Although the vibrational structure of band 5 ($4a_1$) of adamantane was revealed in the high energy-resolution He I UPS,[38c-d] the present PIES in Figure 1 suggests that the Penning ionization process prefers the 0−0 vibrational component (a skeletal and CH_2 scissoring mode), as indicated by the shape of band 5. In contrast to band 5 of adamantane, band 7 ($2a_{2u}$) of cyclohexane shows a more diffuse vibrational structure both in UPS and PIES of Figure 3. Furthermore, the width and peak shift of band 7 in the lower-energy-resolution spectra of Figure 7 exhibit remarkable dependence on the collision energies.

Enhancement of the bands assigned to C_{2s} character in the PIES has been observed for several hydrocarbons containing multiple carbon atoms.[13] In this work, the intensities of bands 5 and 6 of $C_{10}H_{16}$ and bands 7 and 8 of C_6H_{12} are enhanced significantly in the He*(2^3S) PIES. This unusual enhancement in PIES is due to the formation of an excimer-like state that is partly involved in a C_{2s} type hole in the target molecule which facilitates intramolecular Auger-like autoionization almost selectively from orbitals with the C_{2s} character.[13] Moreover, band 8 ($2e_g$ of C_6H_{12}) appears more intense than band 6 ($4t_2$) of $C_{10}H_{16}$, attributable to the smaller energy difference of the $2e_g$ orbital with respect to the inner orbital (φ_i) in electron transfer and the larger magnitude of the overlap between φ_{2e_g} and φ_i.

Typically, negative slopes with negative peak energy shifts represent attractive potentials around certain groups, and positive slopes with positive shifts indicate repulsive potentials. However, the real case is not so simple. Repulsive potentials between σ_{CC} and σ_{CH} bonds and He*(2^3S) were observed frequently.[13-20] We also notice that the slope changes from very positive for $4t_2$ and $3t_2$ of $C(CH_3)_4$[13] to almost flat for 3e′ and 1e″ of cyclopropane.[14] The latter ($m = -0.09$ and -0.08 for 3e′ and $+0.02$ for 1e″) with different peak shifts ($\Delta E = -25$, -65, and $+40$ meV) indicates that there exists a shallow potential well and that the repulsive potential wall is hard for the σ_{CC}

TABLE 4: Band Assignments, Ionization Potentials (IP/eV), Peak Shifts (Δ*E*/meV), and Slope Parameters (*m*) for C_6ClH_{11}

band	orbital character [a]	IP_{obsd}/eV	IP_{OVGF}/eV (pole strength)		$IP_{Koopmans}$/eV[b]		Δ*E*/meV	*m*
			e-C_6ClH_{11}	*a*-C_6ClH_{11}	*e*-C_6ClH_{11}	*a*-C_6ClH_{11}		
1	11a″($n_{Cl}^{\parallel}$,σ_{CCl})	10.46	10.36(0.91)	10.41(0.91)	11.42	11.46	−230 ± 60	−0.37 ± 0.03
	21a′ ($n_{Cl}^{\perp}$)		10.48(0.91)	10.39(0.91)	11.49	11.40		
2	20a′($n_{Cl}^{\parallel}$,σ_{CH})	(11.10)	11.18(0.91)	11.20(0.91)	12.22	12.31	(−150 ± 100)	−0.28 ± 0.03
	10a″($\sigma_{CCl,CC}$)	(11.38)	11.30(0.91)	11.18(0.91)	12.45	12.30		
	19a′(π_{CH},π_{CCl})	(11.94)	11.81(0.92)	11.61(0.92)	12.77	12.57		
3	9a″(π_{CC})	(12.50)	12.52(0.91)	12.45(0.91)	13.61	13.54	(−150 ± 100)	−0.27 ± 0.02
	18a′(σ_{CH},$n_{Cl}^{\parallel}$)		12.85(0.91)	12.45(0.91)	13.95	13.38		
4	17a′($n_{Cl}^{\parallel}$,σ_{CC})	(13.40)	13.29(0.91)	13.70(0.91)	14.51	15.11	(−200 ± 100)	−0.26 ± 0.02
	7a″(σ_{CH},σ_{CC})		13.45(0.91)	13.31(0.90)	14.77	14.65		
	8a″ (σ_{CC},σ_{CH})		13.41(0.90)	13.32(0.91)	14.96	14.85		
5	16a′(σ_{CH}, $n_{Cl}^{\parallel}$)	(15.15)	15.23(0.91)	14.95(0.91)	16.64	16.19	(−20 ± 60)	−0.09 ± 0.04
6	6a″ (σ_{CH})	(15.32)	15.28(0.91)	15.28(0.91)	16.76	16.77	(−200 ± 200)	−0.22 ± 0.02
	15a′ (σ_{CH})		15.43(0.91)	15.61(0.91)	16.92	17.05		
7	14a′ (σ_{CH})	16.39	16.38(0.90)	16.54(0.90)	17.99	18.30	−40 ± 40	−0.07 ± 0.01
8′	13a′(C_{2s},Cl_{3s},σ_{CH})[c]	18.02 [d]				20.24		(−0.14 ± 0.03)
8	13a′(C_{2s},Cl_{3s}, σ_{CH})	18.80 [d]			20.99			−0.17 ± 0.03
9	12a′(C_{2s})	19.75			22.57	22.61		(−0.19 ± 0.03)

[a] The electronic spectra and the orbital characters were assigned with the *e*-C_6ClH_{11}. [b] Calculated at the HF/6-31+G(d,p) level with the B3LYP/6-311++G** optimized geometries. [c] Of the ionic state of *a*-C_6ClH_{11}. [d] The IP values of the 13a′ of *a*-C_6ClH_{11} obtained from the He*(2^3S) PIES.

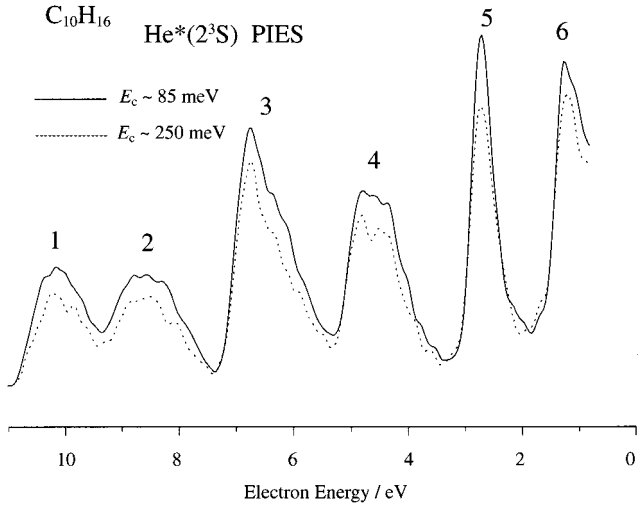

Figure 5. Collision-energy-resolved He*(2^3S) Penning ionization electron spectra of adamantane: solid curve, E_c = 83−87 meV, average 85 meV; dotted curve, E_c = 237−263 meV, average 250 meV.

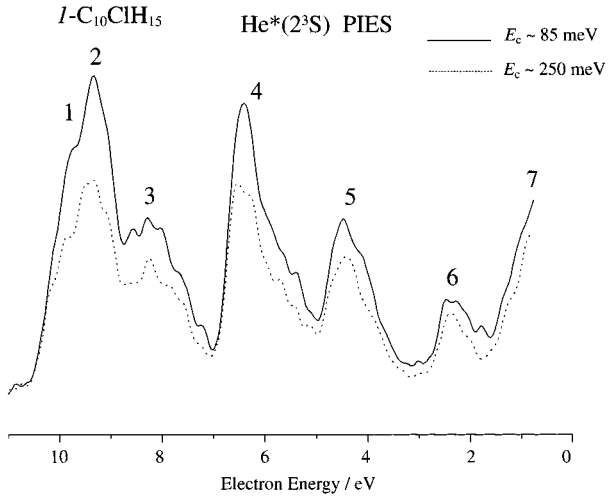

Figure 6. Collision-energy-resolved He*(2^3S) Penning ionization electron spectra of *1*-chloroadamantane: solid curve, E_c = 83−87 meV, average 85 meV; dotted curve, E_c = 238−262 meV, average 250 meV.

bond 3e′, whereas the repulsive wall around hydrogen atoms for 1e″ orbital is softer.[14] Recently, the larger negative slopes were observed for the stronger repulsive interactions for σ_{CC} bonds and CH_2 groups in [2−2]-paracyclophane.[20] Although both adamantane and cyclohexane are purely saturated hydrocarbons, it is surprising to find that all slopes of each band of $C_{10}H_{16}$ and C_6H_{12} are negative. Such negative collision energy dependence is hardly observed for other saturated hydrocarbons. The larger negative slopes for the outer valence bands of $C_{10}H_{16}$ and C_6 H_{12} (in Figures 9 and 11 and Tables 1 and 3) indicate that their repulsive potential walls are extremely hard. This is in good agreement with the calculated potential curves for $C_{10}H_{16}$ and C_6 H_{12} in Figures 13 and 15. In Figure 13, the interaction potential energy of curve A decreases a little more sharply than curves C and D, indicating that repulsive interaction between the C−C bonds and the He* atoms is stronger than between the $C-H_{(2)}$ bonds and the He* atoms. This matches the experimental observations in which the slopes of bands 1 and 2 (mainly with σ_{CC} character) are more negative than those of bands 3 and 4 (mainly with σ_{CH} character) for adamantane. Such features are not so clear for cyclohexane; in Figure 15, the interaction energy in direction A decreases as rapidly as that in direction C, and their slopes are also similar. A minimum point is found in direction B (*R* ca. 1.5 Å for adamantane), but it cannot be observed because it is out of the present experimental energy range (<400 meV). The repulsive interaction in direction B in Figure 15 is much weaker than in the other directions, which is very similar to the situation for cyclopropane.[14] Basic theory regarding the relationships between the calculated potential curves and the experimental CEDPICS will be presented in section C.

B. *1*-Chloroadamantane and Chlorocyclohexane. *1*-$C_{10}ClH_{15}$ has only one stable conformer with C_{3v} symmetry, whereas C_6ClH_{11} exists as equilibrium mixtures of *e* and *a* conformers (both with C_s symmetry) in gas phase, in solution, in liquid state, and in amorphous solids. In all phases, the *e* conformer is in the higher abundance. The ratio of compositions was estimated to be *e*-C_6ClH_{11}:*a*-C_6ClH_{11} = 75(6)%:25(6)% from the gas-phase electron diffraction experiments at the room temperature.[51] In this study, orbitals of *e*-C_6ClH_{11} are employed in the analysis of electron spectra.

Seven bands are assigned in the electron spectra of *1*-$C_{10}ClH_{15}$ in Figure 2. Bands 1 and 2 are due to the lone-pair electrons of the n_{Cl} orbital (14e), σ_{CCl} bonding orbital ($16a_1$),

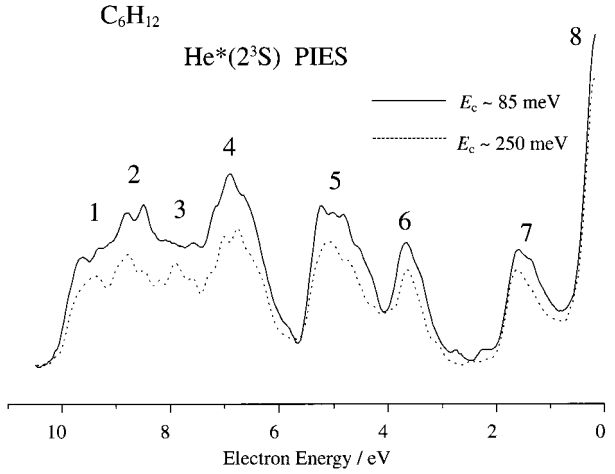

Figure 7. Collision-energy-resolved He*(2^3S) Penning ionization electron spectra of cyclohexane: solid curve, $E_c = 83-87$ meV, average 85 meV; dotted curve, $E_c = 241-259$ meV, average 250 meV.

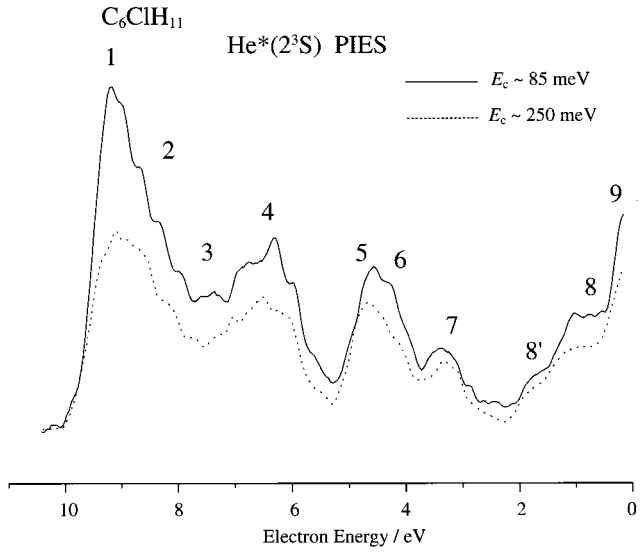

Figure 8. Collision-energy-resolved He*(2^3S) Penning ionization electron spectra of chlorocyclohexane: solid curve, $E_c = 83-87$ meV, average 85 meV; dotted curve, $E_c = 241-259$ meV, average 250 meV.

and 13e with σ_{CH} and n_{Cl} characters. Both m and ΔE for these orbitals are strongly negative. In particular, the largest negative slope ($m = -0.33 \pm 0.03$) is observed for the $16a_1$ and 13e orbitals. It is well-known that the slower He* metastable atom can approach the reactive region effectively by the attractive force to result in an enhanced ionization cross section for the lower collision energy. The negative slope parameter indicates a decrease in ionization reactivity with increasing of collision energy, and this is usually associated with a negative peak energy shift. The region localized by 14e electrons shows strong attractive interaction with He*(2^3S) atoms, whereas the $16a_1$ region shows strong repulsion. The repulsive interactions along the σ_{CCl} bond axis have also been observed for $(CH_3)_3CCl$[13] and C_2H_5Cl[33] with flat slopes, indicating that there may exist softer repulsive interaction along the C−Cl bond axis. As shown in the electron density maps in Figure 10, the main orbital character of 14e is the parallel or perpendicular distribution of the lone-pair electrons. The calculated model potentials in Figure 14 also indicate that there are deep potential wells in the interaction curves for the directions perpendicular to the C−Cl bond axis and a hard potential wall for interaction along the C−Cl bond axis. The calculated curves support the validity of

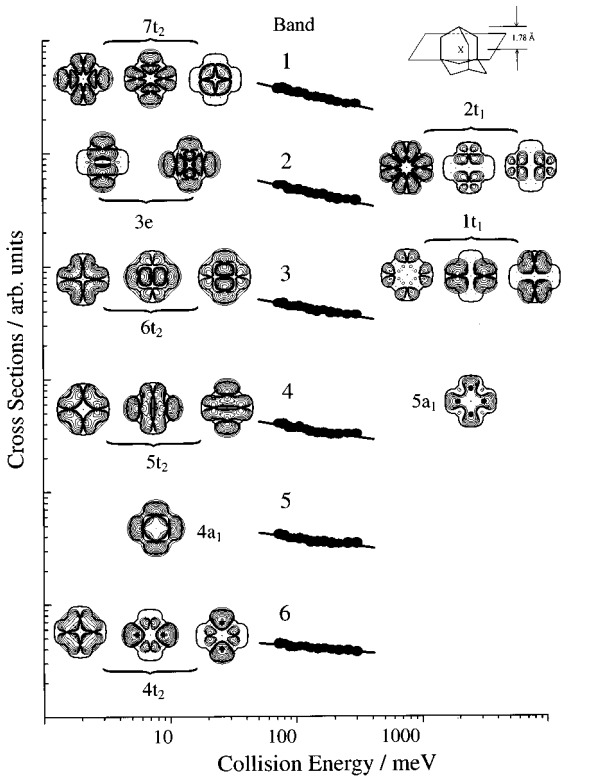

Figure 9. Collision energy dependence of partial ionization cross sections for adamantane collided with He*(2^3S). Electron density maps for respective MOs are also shown on a plane including the center (X) of mass of adamantane.

the above approximation. Although π_{CCl} and n_{Cl} characters are observed for 11e and 12e in band 3, these electrons are mainly associated with σ_{CC} bonding. Therefore, the PIES intensity of band 3 is relatively as low as bands 1 and 2 of $C_{10}H_{16}$ and bands 1, 2, and 3 of C_6H_{12} shown in Figures 1 and 3. Band 3 has a comparable negative slope due to the strong repulsive interaction between the C−C bonds and the He*(2^3S) atom. The high intensities in the PIES and the negative slopes ($m = -0.19 \pm 0.02$ and -0.16 ± 0.04) of bands 6 and 7 can be ascribed to C_{2s}, Cl_{3s}, and σ_{CH} characters. Resonant excitation transfer and the subsequent autoionization can also be expected for these C_{2s} bands.

Assignments in the electron spectra of C_6ClH_{11} are complex due to not only the isomer mixture but also the splitting of doubly degenerate orbitals of C_6H_{12}. The σ_{CCl} bonding may be responsible for the enhanced intensity of band 1 in PIES. For the IPs of the *e* and *a* conformers predicted by the OVGF calculations, the energetic sequence between 21a′ and 11a″ is reversed, and σ_{CCl} is mixed somewhat with n_{Cl} for 11a″ of *e*-C_6ClH_{11} and 21a′ of *a*-C_6ClH_{11}. Therefore, we assign band 1 as having (n_{Cl},σ_{CCl}) character. For bands 2−4, the ionization states overlap seriously in the Penning spectrum (Figure 4). The flat slope of the 16a′ orbital (band 5) indicates that the attractive interaction around the Cl atom is comparable to the repulsive interaction of the weak σ_{CH} bonds. The flatter slope of 14a′ (band 7) also shows that the repulsive interaction for weak σ_{CH} bonding is much weaker than others. A shoulder on the high-electron-energy side of band 8 is assigned as band 8′ to ionization by the 13a′ orbital of *a*-C_6ClH_{11}. This is supported by several points. First, there are ca. 0.8 eV differences in the IPs as predicted by the Koopmans' approximation (see Table 4), which matches the observation of PIES in Figure 4; second, their negative slopes ($m = 0.14 \pm 0.03$ and 0.17 ± 0.03) are

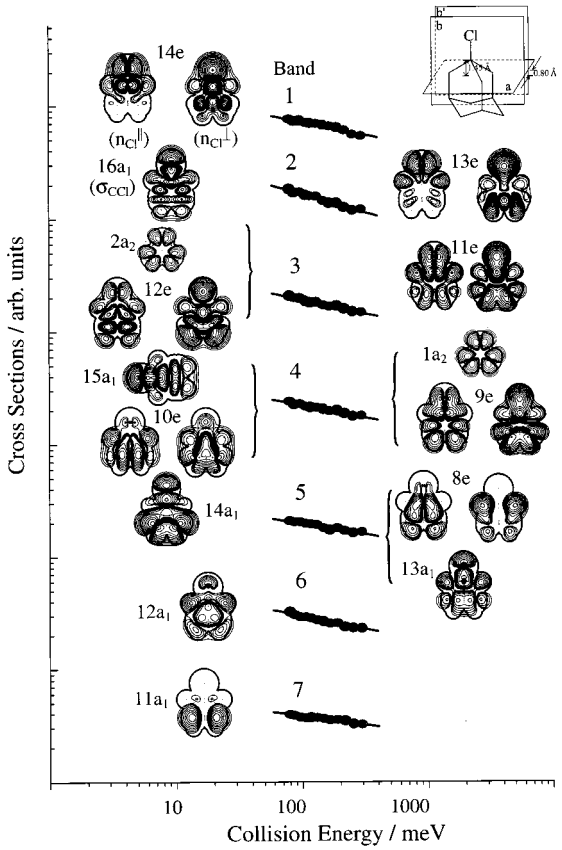

Figure 10. Collision energy dependence of partial ionization cross sections for *1*-chloroadamantane collided with He*(2^3S). Electron density maps are shown on a plane (a) at a distance of 1.45 Å from the C atom bonded to the Cl atom for a_2 orbitals; on a plane (b) where the C−Cl is included, density maps are shown for e (the left maps) and a_1 (except for $14a_1$) orbitals; the right maps of e orbitals and the map of $14a_1$ are shown on a plane b′ which is parallel to b at the distance of 0.80 Å.

similar; and finally, the ratio of peak intensities of the PIES is estimated to be band 8′:band 8 ≈ 1:3, which well matches the composition ratio.[51]

C. CEDPICS and Interaction Potentials. In the previous studies,[14−20,26,30−33,47] simple theoretical models of isotropic systems have been applied effectively for analyzing CEDPICS for molecular systems, even though the molecular systems are usually anisotropic. When the long-range attractive part of the interaction potential $V^*(R)$ plays a dominated role and its function is of the form

$$V^*(R) \propto R^{-s} \tag{8}$$

log $\sigma(E_c)$ can be expressed by

$$\log \sigma(E_c) \propto (-2/s) \log E_c \tag{9}$$

Therefore, the slope of log σ vs log E_c is usually negative ($m = -2/s$). If the repulsive part governs the interaction, log $\sigma(E_c)$ can be derived as

$$\log \sigma(E_c) \propto \left(\frac{b}{d} - \frac{1}{2}\right) \log\left(\frac{E_c}{C}\right) + \log\left[\ln\left(\frac{E_c}{C}\right)^2\right] \tag{10}$$

on the basis of the assumption of simple damped exponential functions of the interaction potential $V^*(R)$ and the electronic transition probability $w(R)$ as follows:

$$V^*(R) = A \exp(-dR)$$
$$w(R) = C \exp(-bR) \tag{11}$$

When the second term in eq 10 is neglected, the slope m of log σ vs log E_c is related to the two parameters b and d in eq 11, the parameter b can be estimated from the lowest IP value of the molecule, and hence the slope parameter m can be determined by

$$m = \frac{b}{d} - \frac{1}{2} = \frac{2(2\mathrm{IP})^{1/2}}{d} - \frac{1}{2} \tag{12}$$

For a given molecule, the m values of different orbitals are only related to the parameter d. Therefore, the parameter d gives the effective steepness of the repulsive potential wall, and it is possible to determine whether the potential wall will be soft, hard, or very hard (d value from smaller, medium, to larger) according to whether the m value is positive, zero, or negative ($m > -0.5$).

According to the discussion at the end of section A, the outer valence orbitals $7t_2$, 3e, and $2t_1$ of $C_{10}H_{16}$ and $4e_g$, $4a_{1g}$, and $4e_u$ of C_6H_{12} have the steeper slopes ($m = -0.23$ to -0.28), while the orbitals $6t_2$, $5t_2$, and $5a_1$ of $C_{10}H_{16}$ have the shallower ones. All exhibit the negative peak shifts except for the $4e_g$ and $4a_{1g}$ orbitals which may show positive shifts that could not be determined accurately because of the diffuseness of bands. Therefore, the repulsive interaction between the σ_{CC} bonds and the He* atoms is stronger than that for the $\sigma_{CH(2)}$ bonds. The orbitals with σ_{CH} bonding character, $3e_u$, $3e_g$, $3a_{2u}$, and $3a_{1g}$ of C_6H_{12}, show the larger negative slopes compared to the corresponding orbitals of $C_{10}H_{16}$. It means that the repulsive interactions between the CH_2 of C_6H_{12} and the He* atom are

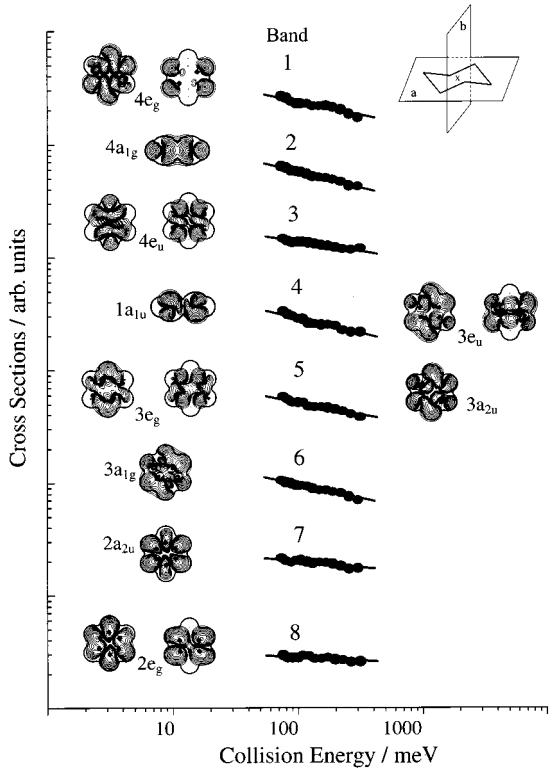

Figure 11. Collision energy dependence of partial ionization cross sections for cyclohexane collided with He*(2^3S). Electron density maps for respective MOs except for $4a_{1g}$ and $1a_{1u}$ are shown on the XY plane (a), and the other two are on the YZ plane (b).

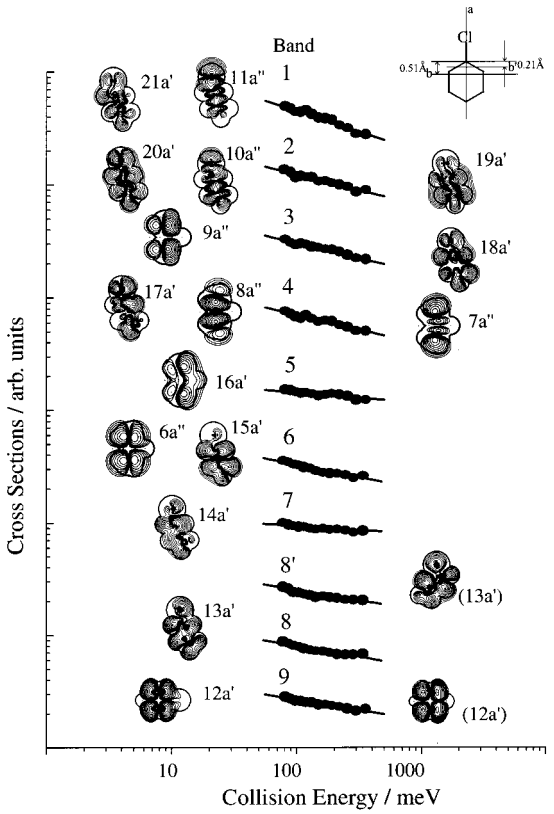

Figure 12. Collision energy dependence of partial ionization cross sections for chlorocyclohexane collided with He*(2^3S). Electron density maps for respective MOs except for 9a″, 8a″, 7a″, 16a′, 6a″, and 12a′ are shown on the molecular plane (a); the maps for 9a″, 8a″, 7a″, 16a′, and 6a″ are shown on a plane (b) which is at a distance of 0.51 Å to the C atom bonded the Cl atom; the map for 12a′ is shown on a plane (b′) which is parallel to plane b and at a distance of 0.21 Å to the C atom. Both plane b and b′ are perpendicular to plane a. The maps for *a* conformer are shown for 13a′ and 12a′ orbitals in parentheses.

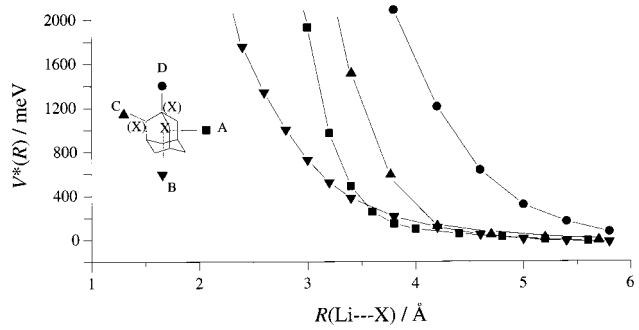

Figure 13. Interaction potential curves $V^*(R)$ for adamantane−Li: (■), along the line crossing the middle of C−C bond and the cage center X; (▲), along the line crossing the C(H_2) or (X) and the cage center X; (●), along the line crossing the C(H) or (X) and the cage center X; (▼), access to the center of a six-carbon ring along a C_3 axis.

stronger and that the repulsive potentials around the CH_2 groups of the larger bulky structure of $C_{10}H_{16}$ are softer. The *d* value of interaction with $CH_{(2)}$ groups for C_6H_{12} is estimated to be ca. 30% larger than that for $C_{10}H_{16}$, based on experimental data and eq 10. Fitting the calculated potential energies in Figures 13 and 15 with the damped exponential function $V^*(R)$ in eq 11 gives a *d* value for C_6H_{12} that is ca. 20% larger than that for $C_{10}H_{16}$. The present model calculations are in good qualitative agreement with the experimental observations. Small negative peak shifts for these strong repulsive interactions can be interpreted as the shallow potential wells far from the molecular surface (the well depth is less than 100 meV for the present

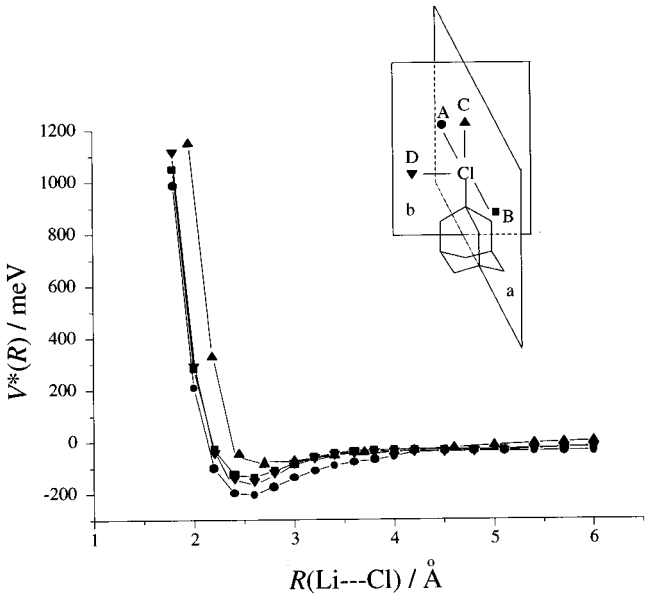

Figure 14. Interaction potential curves $V^*(R)$ for *1*-chloroadamantane-Li: (●) and (■), perpendicular to C−Cl bond in-plane (a); (▲), along the C−Cl bond in-plane (b); (▼), perpendicular to C−Cl bond in-plane (b).

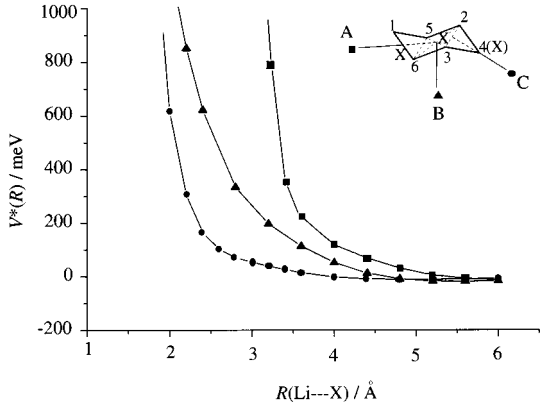

Figure 15. Interaction potential curves $V^*(R)$ for cyclohexane-Li: (●), access to C(H_2) or (X) in-plane (2−3−4); (■), along the line crossing the middle of C−C bond or (X) and the ring center X; (▲), access to in the center X along the central axis.

calculations). Although the peak shifts are estimated with relatively large error, the σ_{CC} and σ_{CH} bands have different peak shifts for adamantane and cyclohexane. It is interesting that bands 1 and 2 for $C_{10}H_{16}$ show negative peak shifts, whereas bands 1 and 2 for C_6H_{12} show the positive ones, and that the reverse occurs for bands 3 and 4 for $C_{10}H_{16}$ and bands 4 and 5 for C_6H_{12}. This also indicates that interactions with the σ_{CC} bonds of $C_{10}H_{16}$ are stronger than those of C_6H_{12}, which is contrary to interactions with σ_{CH} bonds. The stronger repulsive interaction with the σ_{CC} bonds of $C_{10}H_{16}$ indicates that the cage-like adamantane skeleton should interact with the Li atom more rigidly than the cyclohexane ring.

For molecular *1*-$C_{10}ClH_{15}$ and C_6ClH_{11}, strong attractive interactions around the Cl atom are observed. The calculated potential curves are shown in Figures 14 and 16. Deep potential wells exist for the interactions perpendicular to the C−Cl bond axes, and hard walls and shallow wells occur in the C−Cl axial directions. For the attractive interactions, the larger absolute value of the negative *m* corresponds to the smaller *s* value of eq 9; the *s* value for band 1 of *1*-$C_{10}ClH_{15}$ is estimated to be ca. 9.5, whereas that for band 1 of C_6ClH_{11} is ca. 5.5, using the experimental *m* data. The exact value of E_e^i is equal to the

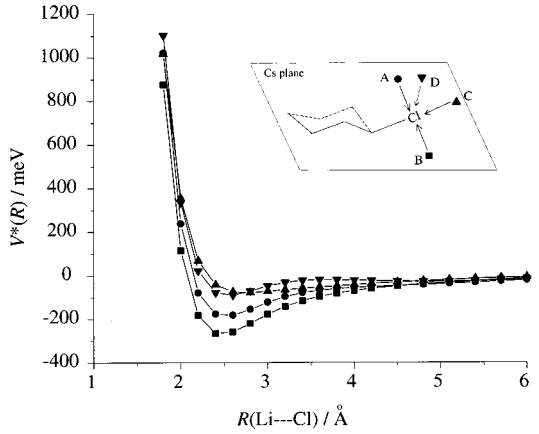

Figure 16. Interaction potential curves $V^*(R)$ for chlorocyclohexane-Li: in the C_s plane, (●) and (■) perpendicular to the C−Cl bond, (▲) along the C−Cl bond; vertical to the C_s plane, (▼) perpendicular to the C−Cl bond.

difference between V^* and V^+. In the fact that the outgoing interaction potential (molecular anion and the ground state atomic He) is usually flat, so the potential well depth of V^* can be estimated via the peak energy shift.[52] In Figures 14 and 16, the potential well depths for the interactions perpendicular to the C−Cl bond are predicted to be ca. 200 and 260 meV for *1*-$C_{10}ClH_{15}$ and C_6ClH_{11}, respectively. These values are in good agreement with those for the corresponding peak shifts (ΔE = 200 ± 140 and 230 ± 60 meV) estimated from the electron spectra in Figures 2 and 4. The relatively small negative slope and peak shift indicate that the attractive interaction perpendicular to the C−Cl bond of *1*-$C_{10}ClH_{15}$ is weaker than that of C_6ClH_{11}. The strength of the attractive interaction around the chlorine atom substituted into the different saturated hydrocarbons will be discussed further in the next section. The interaction potentials in different directions in Figures 14 and 16 also show that the interaction is more attractive when the Li atom is approaching in the A direction for *1*-$C_{10}ClH_{15}$, whereas this holds for direction B in *e*-C_6ClH_{11}.

D. Reactivity of n_{Cl} Orbitals of the Saturated Chloro-Hydrocarbons. Spin−orbit coupling in the Cl lone-pair ionizations are not observed clearly, because the spin−orbit slitting energy is ca. 80 meV which is close to the present experimental energy resolution. The effect of Cl substitution is examined by comparison of the IPs of the lone pair orbital for certain saturated chloro-hydrocarbons (some lone-pair IPs are estimated by averaging the ionization potentials of two peaks observed in better energy-resolved experiments), and for the corresponding saturated hydrocarbons.[41] As shown in Figure 17a, a decrease in the absolute IP(HOMO) values for these saturated hydrocarbons (ethane,[41] propane,[41] isobutane,[41] cyclohexane, and adamantane) and their chloro-derivatives (ethyl chloride,[41] *n*-propyl chloride,[41] *tert*-butyl chloride,[41] chlorocyclohexane, and *1*-chloroadamantane) with increasing alkylation indicates that the introduction of large alkyl groups destabilizes the ground state of the molecule. Moreover, the decrease in IP(n_{Cl}) values of the chloro-derivatives is smaller than that of the parent hydrocarbons. It is noted here that substitution of the Cl atom into adamantane actually stabilizes the molecule by a significant margin (ca. 0.2 eV). Furthermore, the IP(HOMO)s of the hydrocarbons are found to be in a good linear term (as shown in Figure 17b) of the IP differences [ΔIP(HOMO-n_{Cl})] (those are differences between the IP values of the HOMOs of the hydrocarbons and the n_{Cl} orbitals of the related chloro-derivatives). The ΔIP(HOMO-n_{Cl}) increases from negative to positive with an increase of the absolute IP(HOMO) values.

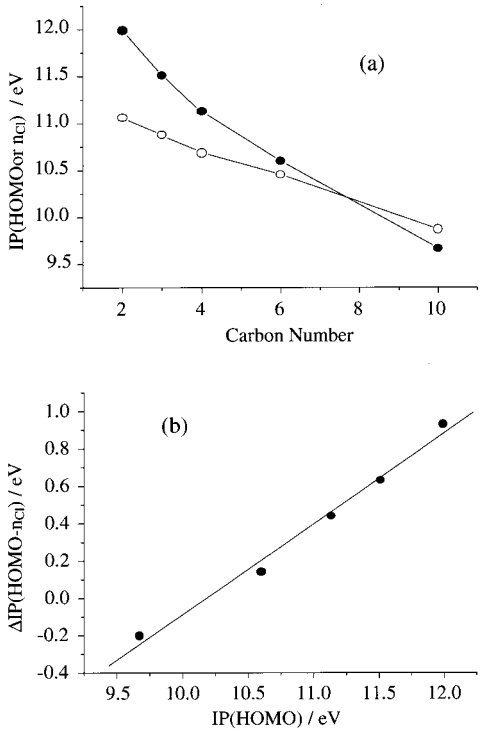

Figure 17. Substitution effect on the lowest ionization potentials: IP(HOMO)s of the saturated hydrocarbons (●) and IP(n_{Cl})s of their chloro-derivatives (○) in (a); correlation (●) between the lowest ionization potential difference ΔIP(HOMO-n_{Cl}) and IP(HOMO), and the least-squares fitted line in (b).

This may be explained by delocalization of the lone-pair electrons of the Cl atoms. The greater alkylation, the more lone-pair electrons are delocalized. The effect of electron delocalization on the n_{Cl} band slopes (m) will be further discussed below.

First, we recall earlier work regarding the effect of HOMO levels (ϵ_{HOMO}) on Penning ionization of substituted ethylenes,[16] where the interaction around the π orbital region becomes more effective for attraction as the ϵ_{HOMO} of the substituted ethylenes becomes higher. The plot of m against ϵ_{HOMO} indicates that the absolute m values increase with a linear step of ca. 0.4 eV^{-1} with ϵ_{HOMO} increasing.[16] The authors also called attention to the fact that interaction around the π orbital region correlates with the capability of electron donation of the substitutent, because the ϵ_{HOMO} reflects the degree of electron donation from the substituent.[16] Therefore, the electron distribution of the π orbital is also related to the attractive interaction. Moreover, it has been noted in a review of PIES that the EED value of individual MO ϕ_i reflects its Penning ionization activity.[24] The slope parameters (m), the EED values, and interaction potential energies[53] for the n_{Cl} orbitals of C_2ClH_5 (C_s), C_4ClH_9 (C_{3v}), *e*-C_6ClH_{11} (C_s), and *1*-$C_{10}ClH_{15}$ (C_{3v}) are plotted against IP(n_{Cl}) in Figure 18. It is surprising that the absolute m value does not increase with IP(n_{Cl}) (approximately equal to $-\epsilon_{HOMO}$) decreasing and that the calculated potential well depths also show a similar tendency. In particular, although the energy level of the n_{Cl} orbital of *1*-$C_{10}ClH_{15}$ is ca. 1.0 eV higher than that of C_2ClH_5, the absolute m value for the former is ca. 0.11 smaller than the latter, which means that the attractivity for the former is weaker than the latter. The EED values of both Cl atom region and total exterior region for the n_{Cl} orbital decrease from the smaller molecule C_2ClH_5 to the larger *1*-$C_{10}ClH_{15}$.

A decrease in the EED values always leads to lower band intensities, which is supported by the experimental observations

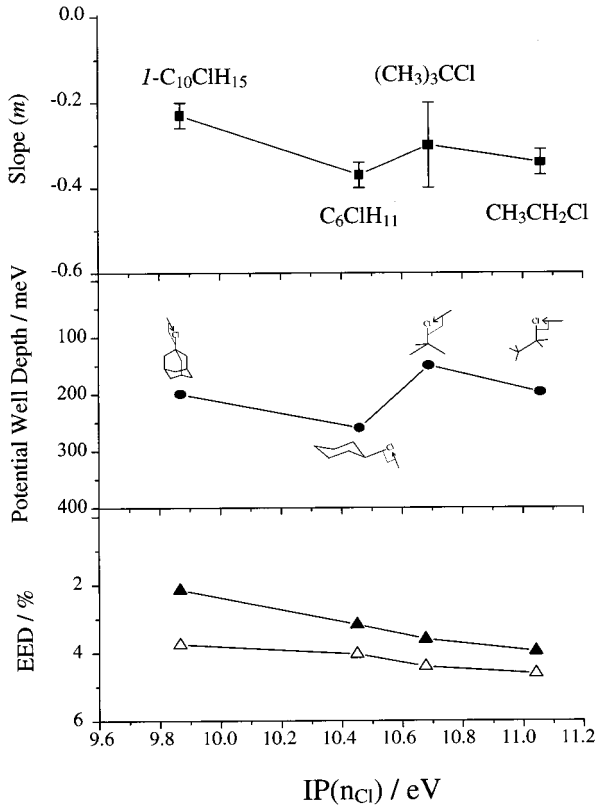

Figure 18. Correlation between IP(n_{Cl}) and the slope parameters *m* of the n_{Cl} orbitals (■ with error bar), potential well depths (meV, ●), and EED values (%, ▲ for the Cl atom region and Δ for the total exterior region of the n_{Cl} orbital).

when we compare the relative intensities in the normal PIES (summarizing all spectra at different collision-energies, as shown in Figures 1−4) for the n_{Cl} bands of C_2ClH_5,[33] C_4ClH_9,[13] *e*-C_6ClH_{11}, and *1*-$C_{10}ClH_{15}$. It further shows that Penning ionization activities for the n_{Cl} bands are decreasing. On the other hand, according to the conclusion in the earlier work,[16] the attractions around the Cl atom should strengthen as their ϵ_{HOMO} becomes higher. This contradiction can be attributed to the fact that a small decrease in the EED values results in a change in the increasing tendency of the absolute *m* values. The less lone-pair electrons in the exterior region, the weaker the attraction around the Cl atom. Moreover, the decrease in the EED value in the Cl atom region (▲) is larger than that of the total orbital region (△) in Figure 18, interpreted as being due to more delocalization of the Cl lone-pair electrons at higher alkylation, which is consistent with the former discussions on IP correlations. In general, the EED value together with ϵ_{HOMO} plays a role in the strength of the anisotropic interaction for a certain group, and the former may in some case become more important.

The similar tendencies of *m* values and potential well depths for C_2ClH_5 to *1*-$C_{10}ClH_{15}$ in Figure 18 also demonstrates that the model potential calculation for interpretation of anisotropic interaction in PIES is reasonable. It is found that the attractivity of perpendicular approaches to the C−Cl axis is decreasing when comparing slope parameters and potential well depths between CH_3CH_2Cl and $(CH_3)_3CCl$, and C_6ClH_{11} and *1*-$C_{10}ClH_{15}$, because of the size of bulky groups into which the Cl atom is substituted. Introduction of the larger group can lead to a reduction in the attraction or more effective delocalization of the Cl lone-pair electrons, which is simply related to the steric shielding effect described previously. However, molecules with identical symmetry can also have different potential well-depths, such as the case of CH_3CH_2Cl and *e*-$C_{11}ClH_{11}$, which may be due to enhancement of n_{Cl} energy levels. In fact, the energy level effect is not as strong as indicated in the earlier observation for the C_s symmetrical ethylenes.[16]

VI. Conclusion

Spectra obtained by Penning ionization electron spectroscopy and He I ultraviolet photoelectron spectroscopy of molecular $C_{10}H_{16}$, *1*-$C_{10}ClH_{15}$, C_6H_{12}, and C_6ClH_{11} are investigated. Spectral assignments are made on the basis of ab initio SCF and outer valence Green's function calculations. In particular, the peak shift of 13a′ in the C_6ClH_{11} spectra due to *e* and *a* isomerism is observed in the range of the higher IP values. Very strong repulsive interaction around the adamantane cage or cyclohexane ring is observed, and the repulsive strength is of the sequence $\sigma_{CC} > \sigma_{CH}$ for these saturated hydrocarbons. Attractive interaction is localized to the perpendicular approach of the He* atom to the C−Cl bond axis. Furthermore, we compare the present IPs and the slope parameters *m* of n_{Cl} orbitals with the data in the literatures[13,33,41] and find that chlorine substitution destabilizes the saturated hydrocarbons of small size but stabilizes the larger ones (a carbon number ≥9 estimated from Figure 17b). The strength of attraction for the n_{Cl} electrons does not increase with the rise of ϵ_{HOMO} of the chloro-hydrocarbons (here HOMO is the n_{Cl} orbital). The IP correlation is interpreted as being due to more effective delocalization of the Cl lone-pair electrons for the larger alkyl introduction; and the attraction strength is considered to be determined by competition between increasing ϵ_{HOMO} and decreasing EED values.

Acknowledgment. This work is partially supported by a Grant in Aid for Scientific Research from the Japanese Ministry of Education, Science and Culture. One of the authors (S.X.T.) thanks the Japan Society for the Promotion of Science (JSPS) for a JSPS Research Fellowship (ID No. 00111). Dr. Igor V. Litvinyuk is acknowledged for supplying the optimized geometry of adamantane.

References and Notes

(1) Penning, F. M. *Naturwissenshaften* **1927**, *15*, 818.
(2) Ḥotop, H.; Niehaus, A. *Z. Phys.* **1969**, *228*, 68.
(3) Čermák, V. *J. Chem. Phys.* **1966**, *44*, 3781.
(4) Niehaus, A. *Adv. Chem. Phys.* **1981**, *45*, 399.
(5) Yencha, A. J. In *Electron Spectroscopy: Theory, Technique and Application*; Brundle, C. R., Baker, A. D., Eds.; Academic Press: New York, 1984; Vol. 5.
(6) Ohno, K.; Mutoh, H.; Harada, Y. *J. Am. Chem. Soc.* **1983**, *105*, 4555.
(7) Dunlavy, D. C.; Martin, D. W.; Siska, P. E. *J. Chem. Phys.* **1990**, *93*, 5347.
(8) Longley, E. J.; Dunlavy, D. C.; Falcetta, M. F.; Bevsek, H. M.; Siska, P. E. *J. Phys. Chem.* **1993**, *97*, 2097.
(9) Siska, P. E. *Rev. Mod. Phys.* **1993**, *65*, 337.
(10) Mitsuke, K.; Takami, T.; Ohno, K. *J. Chem. Phys.* **1989**, *91*, 1618.
(11) Ohno, K.; Takami, T.; Mitsuke, K.; Ishida, T. *J. Chem. Phys.* **1991**, *94*, 2675.
(12) Takami, T.; Ohno, K. *J. Chem. Phys.* **1992**, *96*, 6523.
(13) Takami, T.; Mitsuke, K.; Ohno, K. *J. Chem. Phys.* **1991**, *95*, 918.
(14) Yamakado, H.; Ogawa, T.; Ohno, K. *J. Phys. Chem. A* **1997**, *101*, 3887.
(15) Ohno, K.; Okamura, K.; Yamakado, H.; Hoshino, S.; Takami, T.; Yamauchi, M. *J. Phys. Chem.* **1995**, *99*, 14678.
(16) Yamakado, H.; Okamura, K.; Ohshimo, K.; Kishimoto, N.; Ohno, K. *Chem. Lett.* **1997**, 269.
(17) Yamauchi, M.; Yamakado, H.; Ohno, K. *J. Phys. Chem.* **1997**, *101*, 6184.
(18) Yamauchi, M.; Yamakita, Y.; Yamakado, H.; Ohno, K. *J. Electron Spetrosc. Relat. Phenom.* **1998**, *88*−*91*, 155.
(19) Yamakado, H.; Sawada, Y.; Shinohara, H.; Ohno, K. *J. Electron Spetrosc. Relat. Phenom.* **1998**, *88*−*91*, 927.

(20) Yamakita, Y.; Yamauchi, M.; Ohno, K. *Chem. Phys. Lett.* **2000**, *322*, 189.
(21) Rothe, E. W.; Neynaber, R. H.; Trujillo, S. M. *J. Chem. Phys.* **1965**, *42*, 3310.
(22) Hotop, H. *Radiat. Res.* **1974**, *59*, 379.
(23) (a) Haberland, H.; Lee, Y. T.; Siska, P. E. *Adv. Chem. Phys.* **1981**, *45*, 487. (b) Hotop, H.; Roth, T. E.; Ruf, M.-W.; Yencha, A. J. *Theor. Chem. Acc.* **1998**, *100*, 36.
(24) Ohno, K.; Harada, Y. In *Molecular Spectroscopy, Electronic Structure and Intramolecular Interactions*; Maksić, Z. B., Ed.; Springer-Verlag: Berlin, 1991.
(25) Masuda, S.; Aoyama, M.; Ohno, K.; Harada, Y. *Phys. Rev. Lett.* **1990**, *65*, 3257.
(26) Kishimoto, N.; Yamakado, H.; Ohno, K. *J. Phys. Chem.* **1996**, *100*, 8204.
(27) Tokue, I.; Sakai, Y.; Yamasaki, K. *J. Chem. Phys.* **1997**, *106*, 4491.
(28) Alberti, M.; Lucas, J. M.; Brunetti, B.; Pirani, F.; Stramaccia, M.; Rosi, M.; Vecchiocattivi, F. *J. Phys. Chem. A* **2000**, *104*, 1405.
(29) Yamato, M.; Ohoyama, H.; Kasai, T. *J. Phys. Chem. A* **2001**, *105*, 2967.
(30) Imura, K.; Kishimoto, N.; Ohno, K. *J. Phys. Chem. A* **2001**, *105*, 4189
(31) Ohno, K.; Kishimoto, K.; Yamakado, H. *J. Phys. Chem.* **1995**, *99*, 9687.
(32) Kishimoto, N.; Ohshimo, K.; Ohno, K. *J. Electron Spectrosc. Relat. Phenom.* **1999**, *104*, 145.
(33) Imura, K.; Kishimoto, N.; Ohno, K. *J. Phys. Chem. A* **2001**, *105*, 6378.
(34) Arduengo, A. J., III.; Harlow, R. L.; Kline, M. *J. Am. Chem. Soc.* **1991**, *113*, 361.
(35) (a) Grelak, R.; Clark, R.; Stump, J. M.; Vernier, V. G. *Science* **1970**, *169*, 203. (b) Duvoisin, R. C. *Parkinson's Disease*; Raven Press: New York, 1991; Chapter 6. (c) Margo, K. L.; Shuaghnessy, A. F. *Am. Fam. Physician* **1998**, *57*, 1073.
(36) (a) Lewis, R. T. *Sax's Dangerous Properties of Industrial Materials*, 8th ed.; van Nostrand Reinhold: New York, 1992. (b) Longacre, S. L. *Ethel Browing's Toxicity and Metabolism of Industrial Solvents*, 2nd ed.; Snyder, R., Eds.; Elsevier: Amsterdam, 1987; Volume 1.
(37) (a) Litvinyuk, I. V.; Zheng, Y.; Brion, C. E. *Chem. Phys.* **2000**, *253*, 41. (b) Litvinyuk, I. V.; Zheng, Y.; Brion, C. E. *Chem. Phys.* **2000**, *261*, 289. (c) Litvinyuk, I. V.; Young, J. B.; Zheng, Y.; Cooper, G.; Brion, C. E. *Chem. Phys.* **2001**, *263*, 195.
(38) (a) Bodor, N.; Dewar, M. J. S.; Worley, S. D. *J. Am. Chem. Soc.* **1970**, *92*, 19. (b) Mateescu, G. D.; Worley, S. D. *Tetrahedron Lett.* **1972**, 5285. (c) Schmidt, W. *Tetrahedron* **1973**, *29*, 2129. (d) Boshi, R.; Schimdt, W.; Suffolk, R. J.; Wilkins, B. T. *J. Electron Spectrosc. Relat. Phenom.* **1973**, *2*, 377. (e) Worley, S. D.; Mateescu, G. D.; McFarland, C. W.; Fort, R. C., Jr.; Sheley, C. F. *J. Am. Chem. Soc.* **1973**, *95*, 7580.
(39) (a) Bischof, P. *Helv. Chim. Acta* **1969**, *52*, 1745. (b) Demeo, D. A.; Yencha, A. J. *J. Chem. Phys.* **1970**, *53*, 4536. (c) Ikuta, S.; et al. *Chem. Lett.* **1973**, 1237. (d) Potts, A. W.; Streets, D. G. *J. Chem. Soc., Faraday Trans. 2* **1974**, *70*, 875. (c) Brogli, F.; Heilbronner, E. *Helv. Chim. Acta* **1971**, *54*, 1423.
(40) Gardner, J. L.; Samson, J. A. R. *J. Electron Spectrosc. Relat. Phenom.* **1976**, *8*, 469.
(41) Kimura, K.; Katsumata, S.; Achiba, Y.; Yamazaki, T.; Iwata, S. *Handbook of He I Photoelectron Spectra of Fundamental Organic Molecules*; Japan Scientific: Tokyo, 1981.
(42) Pauling, L. *The Nature of the Chemical Bond*; Cornell University: Ithaca, New York, 1960.
(43) (a) von Niessen, W.; Schirmer, J.; Cederbaum, L. S. *Comput. Phys. Rep.* **1984**, *1*, 57. (b) Zakrzewski, V. G.; Ortiz, J. V. *Int. J. Quantum Chem. Symp.* **1994**, *28*, 23. (c) Zakrzewski, V. G.; Ortiz, J. V. *Int. J. Quantum Chem.* **1995**, *53*, 583.
(44) Frisch, M. J.; Trucks, G. W.; Schlegel, H. B.; Scuseria, G. E.; Robb, M. A.; Cheeseman, J. R.; Zakrzewski, V. G.; Montgomery, J. A., Jr.; Stratmann, R. E.; Burant, J. C.; Dapprich, S.; Millam, J. M.; Daniels, A. D.; Kudin, K. N.; Strain, M. C.; Farkas, O.; Tomasi, J.; Barone, V.; Cossi, M.; Cammi, R.; Mennucci, B.; Pomelli, C.; Adamo, C.; Clifford, S.; Ochterski, J.; Petersson, G. A.; Ayala, P. Y.; Cui, Q.; Morokuma, K.; Malick, D. K.; Rabuck, A. D.; Raghavachari, K.; Foresman, J. B.; Cioslowski, J.; Ortiz, J. V.; Stefanov, B. B.; Liu, G.; Liashenko, A.; Piskorz, P.; Komaromi, I.; Gomperts, R.; Martin, R. L.; Fox, D. J.; Keith, T.; Al-Laham, M. A.; Peng, C. Y.; Nanayakkara, A.; Gonzalez, C.; Challacombe, M.; Gill, P. M. W.; Johnson, B. G.; Chen, W.; Wong, M. W.; Andres, J. L.; Head-Gordon, M.; Replogle, E. S.; Pople, J. A. *Gaussian 98*; Gaussian, Inc.: Pittsburgh, PA, 1998.
(45) Ohno, K.; Matsumoto, S.; Harada, Y. *J. Chem. Phys.* **1984**, *81*, 2183; 4447.
(46) Ohno, K.; Ishida, T.; Naitoh, Y.; Izumi, Y. *J. Am. Chem. Soc.* **1985**, *107*, 8082.
(47) Kishimoto, N.; Yokoi, R.; Yamakado, H.; Ohno, K. *J. Phys. Chem. A* **1997**, *101*, 3284.
(48) Aoyama, M.; Masuda, S.; Ohno, K.; Harada, Y.; Yew, M. C.; Hua, H. H.; Yong, L. S. *J. Phys. Chem.* **1989**, *93*, 1800.
(49) (a) Munakata, T.; Harada, Y.; Ohno, K.; Kuchitsu, K. *Chem. Phys. Lett.* **1981**, *84*, 6. (b) Ohno, K.; Fujisawa, S.; Mutoh, H.; Harada, Y. *J. Phys. Chem.* **1982**, *86*, 440. (c) Harada, Y.; Ohno, K.; Mutoh, H. *J. Chem. Phys.* **1983**, *79*, 3251.
(50) Peters, R. A.; Walker, W. J.; Weber, A. *J. Raman Spectrosc.* **1973**, *1*, 159.
(51) Shen, Q.; Peloquin, J. M. *Acta Chem. Scand. A* **1988**, *42*, 367.
(52) Niehaus, A. *Ber. Bunsen-Ges. Phys. Chem.* **1973**, *77*, 632.

(53) To reduce computational errors, all calculations were performed at the same level of theory. Molecular structures of C_2ClH_5 (C_s) and C_4ClH_9 (C_{3v}) were also optimized at the B3LYP/6-311++G** level. Using the optimized geometries of these four molecules, we calculated the EED values of the Cl atom region (▲) and total exterior region (△) for the n_{Cl} orbitals at the HF/6-31+G* level. Interaction potential calculations were performed with the same method given in section III of the main text, and the most favorable approach directions were determined by distributions of Cl lone-pair electrons.